Optimizing magnetodipolar interactions for synchronizing vortex based spin-torque nano-oscillators

F. Abreu Araujo[*]
Institute of Condensed Matter and Nanosciences, Université catholique de Louvain, Place Croix du Sud 1, 1348 Louvain-la-Neuve, Belgium

A. D. Belanovsky, P. N. Skirdkov, K. A. Zvezdin,[†] and A. K. Zvezdin
A. M. Prokhorov General Physics Institute, RAS, Vavilova, 38 119991 Moscow, Russia and Moscow Institute of Physics and Technology, Institutskiy per. 9, 141700 Dolgoprudny, Russia

N. Locatelli,[‡] R. Lebrun, J. Grollier, and V. Cros
Unité Mixte de Physique CNRS/Thales, Avenue A. Fresnel 1, 91767 Palaiseau and Université Paris-Sud, 91405 Orsay, France

G. de Loubens and O. Klein[§]
Service de Physique de l'État Condensé (CNRS URA 2464), CEA Saclay, 91191 Gif-sur-Yvette, France
(Received 12 November 2014; revised manuscript received 16 June 2015; published 22 July 2015)

We report on a theoretical study of the magnetodipolar coupling and synchronization between two vortex-based spin-torque nano-oscillators (STVOs). In this work we study the dependence of the coupling efficiency on the relative magnetization parameters of the vortices in the system. This study is performed in order to propose an optimized configuration of the vortices for synchronizing STVOs. For this purpose, we combine micromagnetic simulations, the Thiele equation approach, and the analytical macrodipole approximation model to identify the optimized configuration for achieving phase-locking between neighboring oscillators. Notably, we compare vortices configurations with parallel (P) core polarities and with opposite (AP) core polarities. We demonstrate that the AP core configuration exhibits a coupling strength about three times higher than in the P core configuration.

DOI: 10.1103/PhysRevB.92.045419 PACS number(s): 75.70.Kw, 75.78.Cd, 75.78.Fg, 85.75.−d

I. INTRODUCTION

In the last decade great attention has been drawn to the phase-locking phenomena of spin-torque nano-oscillators (STNOs) [1–23]. STNOs are anticipated to be promising devices for submicron-scale microwave synthesizers because of their high emission frequency tunability [24–27]. However, an important issue with such devices regarding their practical realization is their low-output oscillation power and low spectral stability. A possible solution to these issues could be the synchronization of a few STNOs [6,19,21,22,26,28]. Synchronization among multiple auto-oscillators can also be useful in the framework of developing associative memories architectures [29–32]. Previous studies reported on synchronization of STNOs interacting with others via spin waves [25,26,33], exchange coupling [6], electric currents [3,28,34], noisy current injection [19], or via magnetodipolar interaction [21,22,35–41].

Among the various synchronization mechanisms, magnetodipolar coupling is inherent and efficient as emphasized in our previous works [21,22] and also in Refs. [35–41]. In the present study, we focus on the magnetodipolar interaction between two vortex-based STNOs.

Single magnetic vortices in cylindrical dots are characterized by two topological parameters [35]. Chirality (C) determines the curling direction of the in-plane magnetization, such that $C = +1$ ($C = -1$) stands for the counterclockwise (clockwise) direction. The orientation of the vortex core magnetization is described by its polarity (P), which takes a value of $P = +1$ ($P = -1$) for core magnetization aligned (antialigned) with the out-of-plane ($\hat{z}$) axis. The relative configuration of two interacting vortices can then take four nonequivalent states, with identical/opposite chiralities and identical/opposite polarities.

In a previous work [21,22], we studied the capability of two vortex-based STNOs to synchronize through dipolar coupling. In this first approach, we have considered only the case of two vortices with identical polarities and chiralities and already demonstrated the possibility of observing synchronization. In the present study, we show that changing the relative polarity and chirality parameters of the vortices will strongly modify the interaction between the auto-oscillators and may strongly modify the efficiency of synchronization. We conduct a numerical study in which we investigate the synchronization properties for selected combinations of vortex parameters, aiming at sorting the best combinations of the (C, P) parameters to achieve synchronization. We also consider two different electrical connections for the current injection, i.e., parallel and series connections, corresponding, respectively, to current flowing in the same and in the opposite direction in the two STVOs.

[*]abreuaraujo.flavio@gmail.com
[†]Also at Istituto P.M. srl, via Grassi 4, 10138 Torino, Italy.
[‡]Present address: Institut d'Electronique Fondamentale, UMR CNRS 8622, Université Paris-Sud, 91405 Orsay, France.
[§]Present address: SPINTEC, UMR CEA/CNRS/UJF-Grenoble 1/ Grenoble-INP, INAC, 38054 Grenoble, France.

 ©2015 American Physical Society

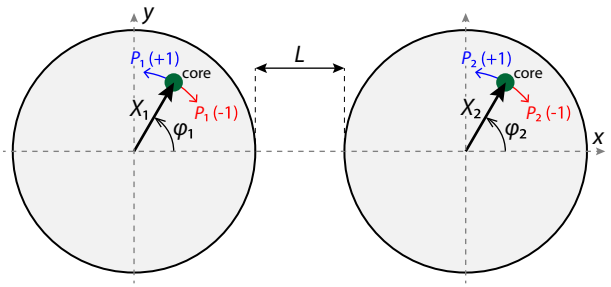


FIG. 1. (Color online) Schematic of the studied system composed of two magnetic dots, each in a magnetic vortex configuration. Vortex cores are shown by filled (green) circles. Vortex core positions are given in polar coordinates, i.e., (X_1,φ_1) and (X_2,φ_2), respectively. Blue arrows, core-up gyrotropic motion sense; red arrows, core-down gyrotropic motion sense.

II. PRESENTATION OF THE SYSTEM

The studied system consists of two circular nanopillars with identical diameters $2R = 200$ nm, separated by an interdot distance L (see Fig. 1). Each incorporates a Permalloy (NiFe) free magnetic layer ($M_s = 800$ emu/cm^3, $A = 1.3\times10^{-6}$ erg/cm, $\alpha = 0.01$) of thickness $h = 10$ nm, separated by an intermediate layer (nonmagnetic metal or tunnel barrier) from a polarizing layer with perpendicular magnetization. Considering their dimensions, each free layer has a magnetic vortex as its remnant magnetic configuration. The vortex parameters are referred to as $P_{1,2}$ and $C_{1,2}$ for the first and second pillars. The polarizing layers, whose magnetizations are identical and oriented along $\hat{z}$, are considered in simulations only through the corresponding current spin polarization $p_{z1} = p_{z2} = p_z = +0.2$. The gyrotropic motion of a vortex core can be driven by spin transfer torque action, by flowing current above a threshold amplitude through each pillar; in our case, the current density $J = 7\times10^6$ A/cm^2 ($I_{DC} = 2.2$ mA). Yet the current sign in each pillar has to be chosen so that $I_i P_i p_z < 0$ to ensure self-sustained oscillations [42,43]. The core polarity of each vortex then defines its gyration direction [44] (see Fig. 1). Indeed, when $P_i = +1$ ($P_i = -1$) the vortex core circular motion is counterclockwise (clockwise).

III. COMBINATIONS OF THE VORTICES TOPOLOGICAL PARAMETERS

We then consider six possible configurations for which self-sustained oscillations are achieved in both pillars, reported in Table I. Note that parallel-core (Pc) configurations correspond to vortices moving in the same direction, whereas antiparallel-core (APc) configurations correspond to vortices moving in opposite directions.

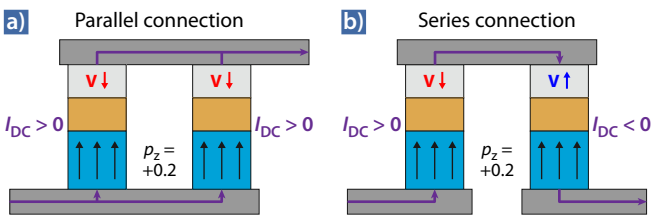


FIG. 2. (Color online) Illustration of the DC supplied current for (a) the Pc and (b) the APc configurations, showing the parallel and series connections, respectively.

TABLE I. Studied configurations with their respective signs of the vortex parameters (C_i, P_i) and current density (J_i).

	Left dot			Right dot		
Config.	C_1	P_1	J_1	C_2	P_2	J_2
Pc1	−1	−1	+	−1	−1	+
Pc2	+1	−1	+	+1	−1	+
Pc3	−1	−1	+	+1	−1	+
APc1	−1	−1	+	+1	+1	−
APc2	+1	−1	+	−1	+1	−
APc3	−1	−1	+	−1	+1	−

Considering the different configurations listed in Table I, the electrical connection must be adapted according to the relative vortex core polarities in order to fulfill the condition $I_i P_i p_z < 0$ to ensure self-sustained oscillations [42,43]. As a consequence, Pc configurations must be alimented using the parallel connection to ensure the same current sign in both pillars [see Fig. 2(a)]. On the contrary, APc configurations have to be supplied with a series connection to ensure opposite current signs [see Fig. 2(b)].

IV. MACRODIPOLE ANALYTICAL MODEL

To get some insights into the origin of the dependence in effective coupling (μ_{eff}) with vortex configuration, we concentrate in this section on an analytical model based on a macrodipole approximation. The dipolar energy (W_{int}) between two magnetic dipoles μ_1 and μ_2 is then given by the following equation (in CGS units):

$$W_{\text{int}} = -\frac{(3(\mu_1\cdot\mathbf{e}_{12})(\mu_2\cdot\mathbf{e}_{12}) - \mu_1\cdot\mu_2)}{\|\mathbf{D}_{12}\|^3}, \qquad (1)$$

where $\mathbf{D}_{12}$ is the vector between the two dipoles and $\mathbf{e}_{12}$ is a unit vector parallel to $\mathbf{D}_{12}$.

Considering two planar dipoles induced by the off-centered vortices in the framework of the two-vortex ansatz (TVA) [45], $\mu_1 = \sigma C_1 X_1(-\sin(\varphi_1), \cos(\varphi_1))$ and $\mu_2 = \sigma C_2 X_2(-\sin(\varphi_2), \cos(\varphi_2))$, where $\sigma = \xi M_s V/R$, $\xi = 2/3$, and $V = \pi R^2 h$. For $\mathbf{D}_{12} = (d,0)$, where $d = 2R + L$ is the interdipole distance along the x axis, and using Eq (1), one obtains

$$W_{\text{int}} = -C_1 C_2 \frac{\sigma^2}{2d^3} X_1 X_2(\cos(\varphi_1 - \varphi_2) - 3\cos(\varphi_1 + \varphi_2)), \qquad (2)$$

where $\dot{\varphi}_i = P_i\omega_i$.

To illustrate the different situations, we consider synchronized oscillations in the two relative polarity configurations. For two vortices with the same core polarity (Pc), gyrating in identical directions at the same frequency $\varphi_1 - \varphi_2 \approx 0$ and $\varphi_1 + \varphi_2 \approx 2\omega_0$, so that Eq. (2) gives

$$W_{\text{int}}^{\text{Pc}} = -C_1 C_2 \frac{\sigma^2}{2d^3} X_1 X_2(1 - 3\cos(2\omega_0 t)). \qquad (3)$$

In contrast, for vortices with opposite polarities (APc), gyrating in opposite directions, $\varphi_1 + \varphi_2 \approx 0$ and $\varphi_1 - \varphi_2 \approx 2\omega_0$,

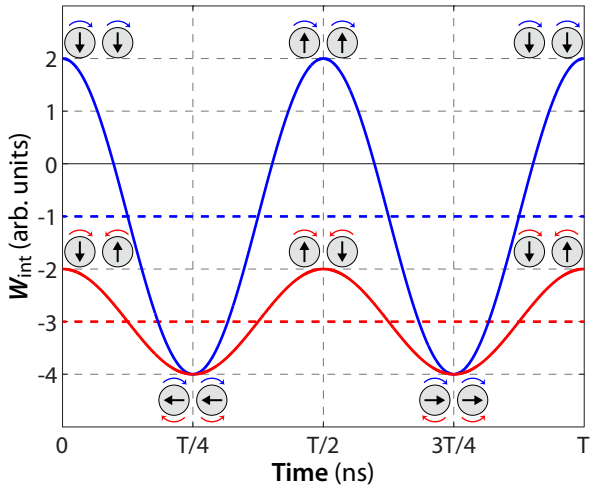


FIG. 3. (Color online) (a) Dipolar energy (W_{int}) evolution of two interacting vortices modeled as macrodipoles and oscillating at the same frequency. The blue curve corresponds to the identical-polarity (Pc) case; the red curve, to the opposite-polarity (APc) case. Dashed colored lines represent the corresponding mean value of the coupling energies $\langle W_{int}\rangle$.

so that one obtains

$$W_{int}^{APc} = -C_1 C_2 \frac{\sigma^2}{2d^3} X_1 X_2 (\cos(2\omega_0 t) - 3). \quad (4)$$

Equations (3) and (4) show that for a given vortex gyration frequency ω_0 the coupling energy W_{int} oscillates at twice the frequency ($2\omega_0$). In the Pc case (see blue curve in Fig. 3) it oscillates with a high amplitude and a small mean value, whereas in the APc case (see red curve in Fig. 3) it oscillates with a low amplitude and a larger mean value.

When not synchronized, the two vortices will feel two oscillating components of the magnetodipolar interaction, i.e., one at low frequency and one at high frequency. The latter one will average out and have a negligible influence on the phase-locking features, while the low-frequency term will be responsible for the synchronization phenomenon. The effective coupling coefficient μ_{eff} can be identified writing $\langle W_{int}\rangle = \mu_{eff} C_1 C_2 X_1 X_2$ for the mean coupling energy and gives the following results for the Pc and APc relative vortex core polarity configurations:

$$\mu_{eff}^{Pc} = -\frac{\pi^2 \xi^2 R^2 h^2}{2d^3},$$
$$\mu_{eff}^{APc} = 3\frac{\pi^2 \xi^2 R^2 h^2}{2d^3}.$$

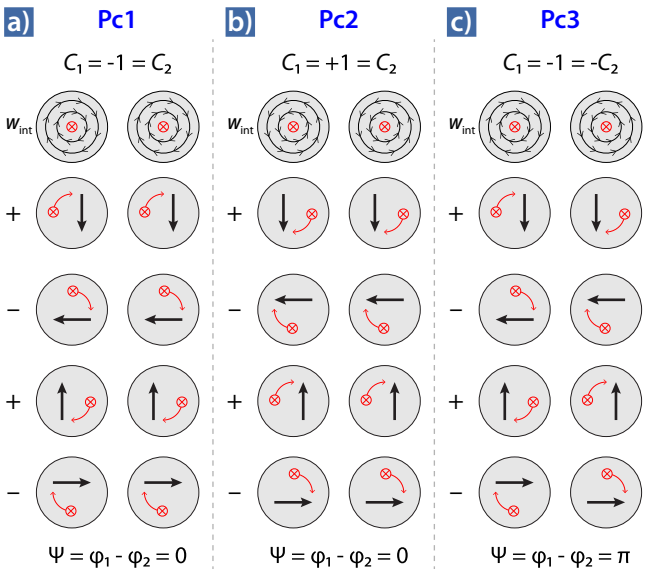


FIG. 4. (Color online) Schematic of the synchronized dynamics for the Pc configurations, i.e., where $P_1 = P_2$.

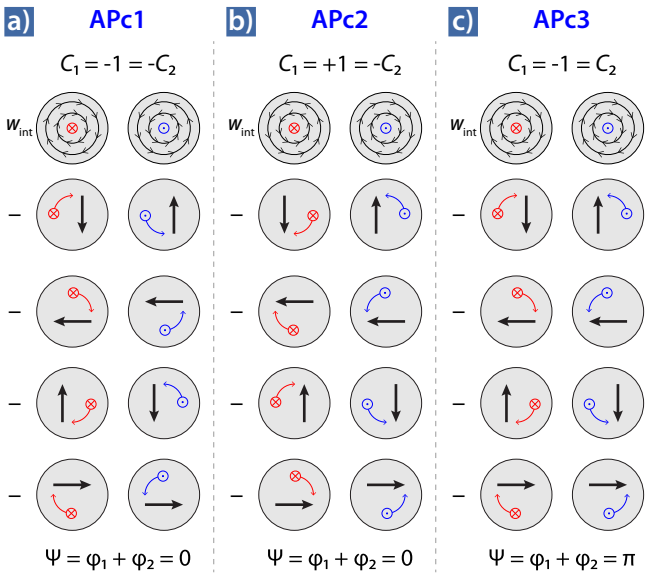


FIG. 5. (Color online) Schematic of the synchronized dynamics for the APc configurations, i.e., where $P_1 = -P_2$.

Synchronized states correspond to a minimization of the average interaction energy. As illustrated here, relative polarity and chirality signs influence the sign of W_{int}. As a consequence, these relative parameters also define the phase relationship achieved when synchronization occurs. The latter considerations are illustrated in Figs. 4 and 5.

From this study, we then conclude that the effective coupling coefficient is predicted to be three times stronger when polarities are opposite (APc) than when polarities are identical (Pc). Concurrently, the high-frequency oscillation of the interaction energy is three times larger in the Pc polarity configuration compared to the APc case. While this indicates that APc is the optimal configuration for synchronization, we must note that this second contribution may affect the locking phenomenon.

V. THIELE ANALYTICAL APPROACH

The spin-transfer-induced gyrotropic vortex dynamics can also be described by the Thiele equation approach [21,43,46,47]:

$$P_i \mathbf{G}_i \times \dot{\mathbf{X}}_i + \mathbf{D}_i \cdot \dot{\mathbf{X}}_i - k_i(X_i, C_i, J_i)\mathbf{X}_i - \mathbf{F}_i^{STT}(p_{zi}, J_i, P_i) - \mathbf{F}_{int}(\mathbf{X}_j, P_i P_j, C_i C_j) = \mathbf{0}, \quad (5)$$

where $\mathbf{G}_i = -G\hat{\mathbf{z}}$ is the gyrovector with $G = 2\pi M_s h/\gamma$ and $\mathbf{D}_i = \alpha\eta_i G$ is the damping coefficient with $\eta_i = 0.5\ln(R_i/(2L_{ex})) + 3/8$ [43], where L_{ex} is the exchange length. For each pillar, the vortex frequency [48,49] is given by the ratio between the confinement coefficient k_i and the gyrovector $\omega_{0|i} = k_i/G$, with

$$k_i(X_i, C_i, J_i) = k_i^{ms} + k_i^{Oe} C_i J_i + \left(k_i'^{ms} + k_i'^{Oe} C_i J_i\right)\left(\frac{\mathbf{X}_i^2}{R_i^2}\right), \tag{6}$$

where k_i^{ms} and $k_i'^{ms}$ (k_i^{Oe} and $k_i'^{Oe}$) correspond to the magnetostatic (Oersted field) contribution. The Oersted contribution will increase the vortex core gyration frequency if the vortex chirality is along the same direction as the Oersted field ($C_i J_i > 0$) and, respectively, decrease the frequency otherwise [50]. Gyration amplitudes will also be affected by such interaction with the Oersted field. To maximize the symmetry of the system and avoid the Oersted contribution's bringing an offset between the two STNO frequencies, we find that the condition $C_1 J_1 C_2 J_2 > 0$ should be ensured (corresponding to identical Oersted contributions in both pillars). This excludes configurations Pc3 and APc3 from Table I from being optimal configurations for synchronization.

The fourth term in Eq. (5) is the spin transfer force, which, for the case of a perpendicularly uniform magnetized polarizer, is written [43]

$$\mathbf{F}_i^{STT} = \kappa(\mathbf{X}_i \times \hat{\mathbf{z}}), \tag{7}$$

where $\kappa = \pi\gamma a_J M_s h$ is the effective spin torque efficiency on the vortex and $a_J = \hbar p_z PJ/(2|e|hM_s)$. In this study, we chose to neglect the field-like torque (FLT) contribution. While the FLT is negligible in the case of a metallic intermediate layer, its amplitude can reach a significant fraction of the Slonczewski torque in the case of a magnetic tunnel junction [51]. However, micromagnetic simulations computed with an FLT contribution of 10% (typical) of the magnitude of the Slonczewski term showed no significant influence on the gyrotropic dynamics. A final term accounts for the interaction dipolar force between the two neighbored vortices, $\mathbf{F}_{int,ji}(\mathbf{X}_{1,2}) = -\partial\langle W_{int}\rangle(\mathbf{X}_1,\mathbf{X}_2)/\partial\mathbf{X}_{1,2} = -C_1 C_2 \mu_{eff}\mathbf{X}_{2,1}$, where μ_{eff} is either μ_{eff}^{P} or μ_{eff}^{AP}, depending on the P_1P_2 sign.

The system of coupled equations for the vortex core motion given in Eq. (5) provides a dynamical description of the phase locking between the two cores. We introduce the two variables $\Psi = P_1\varphi_1 - P_2\varphi_2$ and $\epsilon = (X_1 - X_2)/(X_1 + X_2)$. Following the methodology described by Belanovsky *et al.* [21], by linearizing the system around equilibrium trajectories, we obtain a linear set of equations describing the evolution in time of the relative phases and amplitudes,

$$\dot{\varepsilon} = -2\alpha\eta\left(\frac{\mu_{eff}}{G} + \omega_0 a r_0^2\right)\varepsilon - \frac{\mu_{eff}}{G}\Psi, \tag{8a}$$

$$\dot{\Psi} = -4\left(\frac{\mu_{eff}}{G} + \omega_0 a r_0^2\right)\varepsilon + 2\alpha\eta\frac{\mu_{eff}}{G}\Psi, \tag{8b}$$

where $r_0 = X_0/R$ is the normalized average gyration radius and $a = k'_{ms}/k_{ms} = 1/4$. The two equations (8a) and (8b) are linear and their eigenvalues are

$$\lambda_{1,2} = -\alpha\eta\omega_0 a r_0^2 \pm \sqrt{\alpha^2\eta^2\omega_0^2\left(a r_0^2\right)^2 + 4\frac{\mu_{eff}^2}{G^2} - 4\frac{\mu_{eff}}{G}\omega_0 a r_0^2}.$$

In the case of periodic solutions, the phase-locking dynamics is characterized by a phase-locking time (τ) and a beating frequency (Ω) that can be written as

$$1/\tau = -\alpha\eta\omega_0 a r_0^2, \tag{9a}$$

$$\Omega^2 = -\left(\alpha\eta\omega_0 a r_0^2\right)^2 - 4\left(\frac{\mu_{eff}}{G}\right)^2 - 4\frac{\mu_{eff}}{G}\omega_0 a r_0^2. \tag{9b}$$

In the next section, we propose to realize micromagnetic simulations [52], from which Ω and τ is extracted from the phase-locking dynamics. The effective coupling coefficient in each configuration μ_{eff} is then be derived for each considered configuration by simply reverting Eqs. (9a) and (9b):

$$\mu_{eff}(\tau,\Omega) = \frac{G}{2}\left(1/(\tau\alpha\eta) - \sqrt{1/(\tau\alpha\eta)^2 - \Omega(L)^2}\right). \tag{10}$$

These micromagnetic simulations represent a realistic picture of the coupled system, as they take into account the nonpunctual geometry of the magnets as well as the full current-induced Oersted-field contribution, including cross-talk between nanopillars.

VI. MICROMAGNETIC SIMULATIONS

We first compare the results of micromagnetic simulations obtained for the two cases Pc1 and APc1 with a separating distance between nanopillars $L = 50$ nm. The evolution of radii and dephasing parameter Ψ is shown in Figs. 6(a) and 6(b), respectively, and some numerical values are listed in Table II. These results first confirm that phase-locking is achieved in both configurations. For both configurations, self-sustained unlocked oscillations in each pillar start at the same frequency, but with a random phase shift, and then converge towards a phase-locked regime in almost-identical phase-locking times

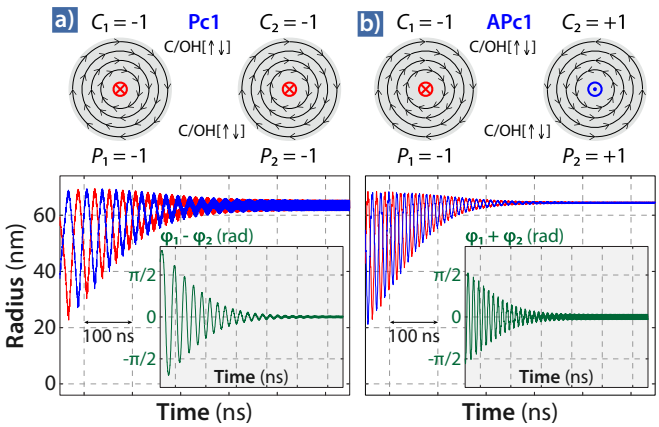


FIG. 6. (Color online) Vortex core orbital radii and (a) phase difference $\Psi = \varphi_1 - \varphi_2$ and (b) sum $\Psi = \varphi_1 + \varphi_2$ obtained by micromagnetic simulations for the Pc1 and APc1 configurations, respectively, where $L = 50$ nm. As shown at the top the chirality (C) is opposite to the Oersted field (OH) in all the dots (C/OH[↑↓]).

TABLE II. Numerical values of parameters extracted from micromagnetic simulations: f is the common oscillation frequency, X_{01} (X_{02}) is the left (right) dot vortex steady-state radius, and Ψ is the dephasing parameter.

Config.	f (MHz)	X_{01} (nm)	X_{02} (nm)	Ψ
Pc1	468.80	63.59	63.59	$\to 0$
APc1	470.57	64.46	64.46	$\to 0$
APc2	497.75	44.51	44.51	$\to 0$
APc3	476.31	65.59	40.59	$\to \pi$

(τ). In their phase-locked state, both vortex cores oscillate with identical radii.

The phase dynamics obtained by micromagnetic simulations are fitted to $\Psi = Ae^{-t/\tau}\sin(\Omega t + \varphi_0)$ to extract Ω, the beating frequency, and τ, the convergence time for phase-locking (see Table III). The effective coupling values for $L = 50$ nm are then deduced: $\mu_{\text{eff}}/G = 19.7$ MHz for the Pc configuration and $\mu_{\text{eff}}/G = 49.2$ MHz for the APc one. The coupling strength then appears to be stronger in the AP configuration ($\sim 2.5\times$) as expected from the macrodipole model.

The results for the "APc2" and the "APc3" configurations for $L = 50$ nm are shown in Fig. 7. Again, in both cases phase-locking is achieved. In the symmetric case APc2, for which both chiralities are parallel to the Oersted field, the starting frequencies are again identical in each pillar, whereas this is not the case for the APc3 configuration, in which symmetry is broken by the Oersted field's being opposed to chirality in only one pillar. In the latter case, the two auto-oscillators have to adapt their frequencies to achieve synchronization to a common frequency $f_1 = f_2 = 476.31$ MHz, by shifting their amplitudes accordingly. As highlighted previously, the micromagnetic simulations confirm that the equilibrium phase shift changes from $|\Psi| = 0$ to $|\Psi| = \pi$ when the sign of the respective chiralities sign(C_1C_2) changes.

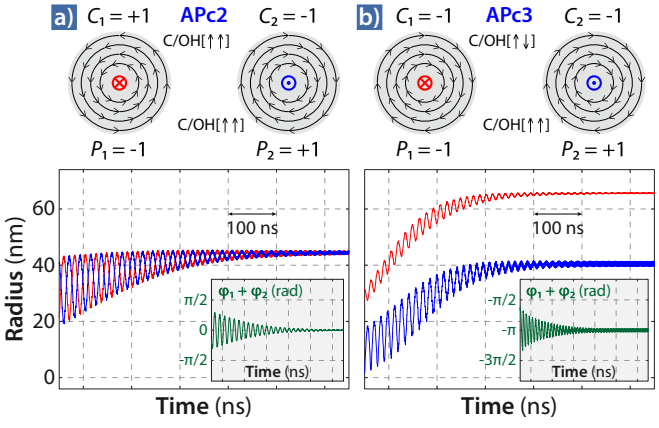


FIG. 7. (Color online) Vortex core orbital radii and phase sum $\Psi = \varphi_1 + \varphi_2$ where $L = 50$ nm for configurations (a) "APc2," where both the vortex chiralities are aligned with the Oersted field (C/OH[↑↑]), and (b) "APc3," where the vortex in the right (left) dot has an antialigned (aligned) chirality with the current-induced Oersted field C/OH[↑↓] (C/OH[↑↑]).

TABLE III. Numerical values of τ, Ω, μ_{eff}/G, and $\langle W_{\text{int}}\rangle$ obtained after combining micromagnetic simulations and our Thiele equation approach for Pc1 and APc1 configurations. The last column, listing the mean interaction energy computed by Eq. (10), also lists the numerical evaluation using Eq. (11) in brackets.

Config.	τ (ns)	Ω (MHz)	μ_{eff}/G (MHz)	$\langle W_{\text{int}}\rangle$ ($\times 10^{-14}$ erg)
Pc1	82.78	40.136	19.7	−22.75 [−27.08]
APc1	71.20	67.380	49.2	−58.31 [−64.23]

VII. NUMERICAL APPROACH

To investigate further the difference in coupling strength between Pc and APc configurations, and validate the macrodipole approach, a more precise numerical calculation of the dipolar energy is proposed. The dipolar interaction energy is here summed up over the full magnetization distributions obtained by micromagnetic simulations. It consists in taking into account all the spin-to-spin, i.e., cell-to-cell, interactions between the left pillar and the right pillar as

$$W_{\text{int}}^{\text{num}} = \sum_{i=1}^{N_1}\sum_{j=1}^{N_2} W_{\text{int},ij}, \tag{11}$$

where $W_{\text{int},ij} = -(3(\mu_i \cdot \mathbf{e}_{ij})(\mu_j \cdot \mathbf{e}_{ij}) - \mu_i \cdot \mu_j)/\|\mathbf{D}_{ij}\|^3$. N_1 (N_2) is the number of cells in the left (right) dot.

As illustrated in Fig. 8 each dot can be seen as being composed of two distinct regions: the outer part (OP) and the inner part (IP) with respect to the vortex gyrotropic trajectory. The OP is a quasistatic region and the IP can be considered an oscillating dipole. The OP contribution is neglected, as it does not contribute to the dynamical coupling. Indeed, as shown in Fig. 10 the values of $\langle W_{\text{int}}^{\text{num}}\rangle$ are close to the values of $\langle W_{\text{int}}\rangle$ obtained through the macrodipole and Thiele equation approach when the OP region is neglected.

Figure 9 shows the results for an edge-to-edge distance between two STVOs of $L = 50$ nm for the APc1 configuration [(red) triangles] and Pc1 configuration [filled (blue) circles]. The dashed lines give the mean value of the interacting dipolar energy $\langle W_{\text{int}}^{\text{num}}\rangle$. In both cases and as expected, the energy $W_{\text{int}}^{\text{num}}$ oscillates at a frequency that corresponds to twice the gyrotropic frequency (see Table II).

We reproduced the process for several other distances between the dots ($L = 100$, 200, and 500 nm). The evolution

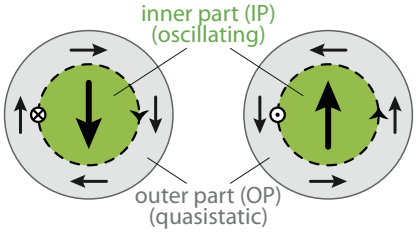


FIG. 8. (Color online) Illustration of the in-plane magnetization of the two oscillating vortices. The outer (gray) zone represents quasistatic magnetization [outer part (OP); $r > X_0$]; the inner (green) zone, oscillating magnetization [inner part (IP); $r < X_0$]. Dashed lines show the vortex orbital movement delimitation where $r = X_0$.

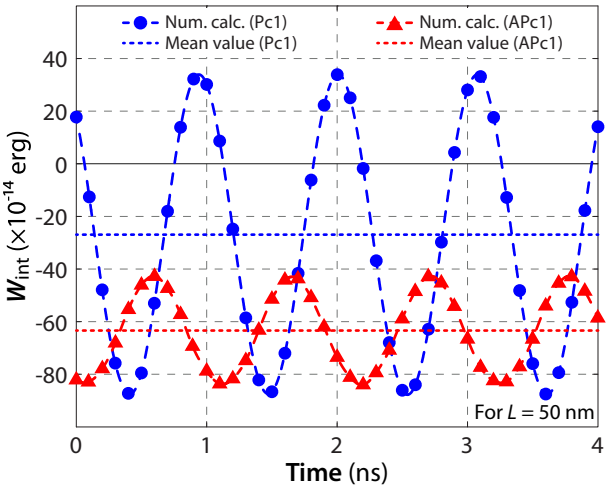


FIG. 9. (Color online) Numerical computation of the dipolar energy ($W_{\rm int}^{\rm num}$) evolution of two interaction and synchronized vortices extracted from micromagnetic simulations for $L = 50$ nm considering the IP region only (see Fig. 8). The dashed (blue) curve shows the evolution of the in-phase oscillating vortices (with parallel polarities, Pc1 configuration); the solid (red) curve, the antiphase case (vortices with antiparallel polarities, APc1 configuration). Dotted colored lines represent the corresponding mean values of the coupling energies ($\langle W_{\rm int}^{\rm num}\rangle$).

of the average interaction energy versus L extracted from micromagnetic simulations is shown in Figs. 10 and 11 for both Pc and APc configurations. The agreement between numerical and Thiele-based estimations of the interacting energy is fairly good, notably for a large interdot distance as shown in Fig. 10. The interaction energy is much higher when the OP and the IP regions are both considered (see Fig. 11).

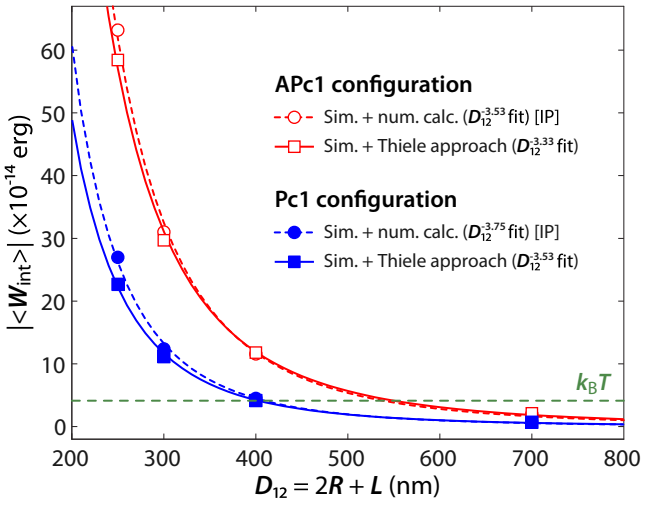


FIG. 10. (Color online) Interdot distance ($D_{12} = 2R + L$) dependence of the absolute value of the mean coupling energy $\langle W_{\rm int}\rangle$: The case for parallel (antiparallel) polarities using a macrodipole and Thiele equation approach model [filled squares (open squares)] and by numerical dipole-dipole computation of the inner parts (IPs; see Fig. 8) of the vortex core trajectories [filled circles (open circles)] are shown in blue (red).

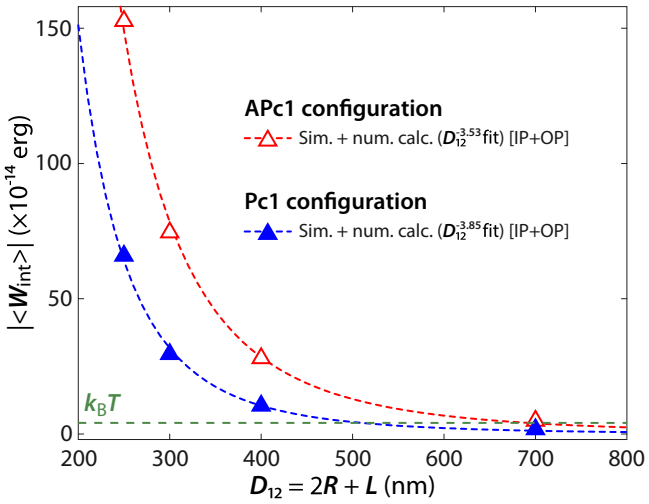


FIG. 11. (Color online) Interdot distance ($D_{12} = 2R + L$) dependence of the absolute value of the coupling energy ($W_{\rm int}$): The case for parallel (Pc) [antiparallel (APc)] polarities obtained by numerical dipole-dipole computation for the whole volume (IP+OP) [filled triangles (open triangles)] are shown in blue (red).

As discussed theoretically in Sec. IV, the macrodipole model gives a ratio of 3 between the interaction energy for the P and that for the AP core configurations. In contrast to that prediction, it should be noted that for small values of the edge-to-edge interdot distance L the ratio between the calculated energies gets lower ($\sim$2.6 for $L = 50$ nm).

The thermal fluctuations were not involved in our simulations. Yet the obtained mean coupling energy $|\langle W_{\rm int}\rangle|$ can be easily compared against the thermal energy ($k_{\rm B}T$). The conditions for stable synchronization, i.e., $|\langle W_{\rm int}\rangle| > k_{\rm B}T$, are then found to be $D_{12} < 400$ nm in the Pc1 configuration and $D_{12} < 550$ nm in the APc1 configuration.

VIII. CONCLUSION

In conclusion, we have performed a comparative study of vortex parameter configurations for the synchronization of two dipolarly coupled spin transfer vortex-based oscillators. As the major result of this numerical and analytical study, we demonstrate that the effective coupling of two vortices with opposite core polarities and hence gyrating in opposite directions is larger than in the case of identical polarities.

By studying different contributions to the coupled vortex dynamics, we have also shown that this configuration matches with feasible experimental configurations. The optimal configuration then corresponds to nanopillars connected in series.

Comparing the computed $W_{\rm int}$ (IP only) with the thermal energy $k_{\rm B}T$, one obtains that synchronization can presumably be achieved at $D_{12} \leqslant 400$ nm, in the case of the parallel polarity configuration (Pc), while $D_{12} \leqslant 550$ would be sufficient in the case of antiparellel polarities.

As far as phase-locking stability is concerned, we highlighted that the dipolar interaction continues to involve strong oscillations in the coupling energy even after achieving synchronization. These interactions will play against synchronization and should decrease the minimum interpillar distance to achieve synchronization.

ACKNOWLEDGMENTS

F.A.A. acknowledges the Research Science Foundation of Belgium (FRS-FNRS) for financial support (FRIA grant) and the UCL for an FSR complement (Fonds Spécial de Recherche). The authors also acknowledge the ANR agency (SPINNOVA ANR-11-NANO-0016) and an EU FP7 grant (MOSAIC No. ICT-FP7-n.317950) for financial support. This publication is based on work funded by Skolkovo Institute of Science and Technology (Skoltech) within the framework of the Skoltech/MIT Initiative. Finally, A.D.B. acknowledges the Dynasty Foundation for financial support.

[1] A. N. Slavin and V. S. Tiberkevich, Nonlinear self-phase-locking effect in an array of current-driven magnetic nanocontacts, Phys. Rev. B **72**, 092407 (2005).

[2] A. N. Slavin and V. S. Tiberkevich, Theory of mutual phase locking of spin-torque nanosized oscillators, Phys. Rev. B **74**, 104401 (2006).

[3] J. Grollier, V. Cros, and A. Fert, Synchronization of spin-transfer oscillators driven by stimulated microwave currents, Phys. Rev. B **73**, 060409 (2006).

[4] S. M. Rezende, F. M. de Aguiar, R. L. Rodríguez-Suárez, and A. Azevedo, Mode locking of spin waves excited by direct currents in microwave nano-oscillators, Phys. Rev. Lett. **98**, 087202 (2007).

[5] B. Georges, J. Grollier, V. Cros, and A. Fert, Impact of the electrical connection of spin transfer nano-oscillators on their synchronization: An analytical study, Appl. Phys. Lett. **92**, 232504 (2008).

[6] A. Ruotolo, V. Cros, B. Georges, A. Dussaux, J. Grollier, C. Deranlot, R. Guillemet, K. Bouzehouane, S. Fusil, and A. Fert, Phase-locking of magnetic vortices mediated by antivortices, Nat. Nano **4**, 528 (2009).

[7] R. Bonin, G. Bertotti, C. Serpico, I. D. Mayergoyz, and M. d'Aquino, Analytical treatment of synchronization of spin-torque oscillators by microwave magnetic fields, Eur. Phys. J. B **68**, 221 (2009).

[8] X. Chen and R. H. Victora, Phase locking of spin-torque oscillators by spin-wave interactions, Phys. Rev. B **79**, 180402 (2009).

[9] A. Slavin, Microwave sources: Spin-torque oscillators get in phase, Nat. Nano **4**, 479 (2009).

[10] V. S. Tiberkevich, A. N. Slavin, E. Bankowski, and G. Gerhart, Phase-locking and frustration in an array of nonlinear spin-torque nano-oscillators, Appl. Phys. Lett. **95**, 262505 (2009).

[11] Y. Zhou and J. Åkerman, Perpendicular spin torque promotes synchronization of magnetic tunnel junction based spin torque oscillators, Appl. Phys. Lett. **94**, 112503 (2009).

[12] P. Tabor, V. S. Tiberkevich, A. N. Slavin, and S. Urazhdin, Hysteretic synchronization of nonlinear spin-torque oscillators, Phys. Rev. B **82**, 020407 (2010).

[13] S. Urazhdin, P. Tabor, V. S. Tiberkevich, and A. Slavin, Fractional synchronization of spin-torque nano-oscillators, Phys. Rev. Lett. **105**, 104101 (2010).

[14] H. Chen, J. Chang, and C. Chang, Synchronization of spin-torque nano-oscillators from an induced corrugated attractor, SPIN **01**, 1 (2011).

[15] D. Li, Y. Zhou, B. Hu, and C. Zhou, Coupled perturbed heteroclinic cycles: Synchronization and dynamical behaviors of spin-torque oscillators, Phys. Rev. B **84**, 104414 (2011).

[16] M. d'Aquino, C. Serpico, R. Bonin, G. Bertotti, and I. D. Mayergoyz, Thermally induced synchronization and stochastic resonance between magnetization regimes in spin-transfer nano-oscillators, J. Appl. Phys. **111**, 07C915 (2012).

[17] G. Finocchio, M. Carpentieri, A. Giordano, and B. Azzerboni, Non-adlerian phase slip and nonstationary synchronization of spin-torque oscillators to a microwave source, Phys. Rev. B **86**, 014438 (2012).

[18] D. Li, Y. Zhou, B. Hu, J. Åkerman, and C. Zhou, Multiple synchronization attractors of serially connected spin-torque nanooscillators, Phys. Rev. B **86**, 014418 (2012).

[19] K. Nakada, S. Yakata, and T. Kimura, Noise-induced synchronization in spin torque nano oscillators, J. Appl. Phys. **111**, 07C920 (2012).

[20] S. Jain, V. Novosad, F. Y. Fradin, J. E. Pearson, V. Tiberkevich, A. N. Slavin, and S. D. Bader, From chaos to selective ordering of vortex cores in interacting mesomagnets, Nat. Commun. **3**, 1330 (2012).

[21] A. D. Belanovsky, N. Locatelli, P. N. Skirdkov, F. Abreu Araujo, J. Grollier, K. A. Zvezdin, V. Cros, and A. K. Zvezdin, Phase locking dynamics of dipolarly coupled vortex-based spin transfer oscillators, Phys. Rev. B **85**, 100409(R) (2012).

[22] A. D. Belanovsky, N. Locatelli, P. N. Skirdkov, F. Abreu Araujo, K. A. Zvezdin, J. Grollier, V. Cros, and A. K. Zvezdin, Numerical and analytical investigation of the synchronization of dipolarly coupled vortex spin-torque nano-oscillators, Appl. Phys. Lett. **103**, 122405 (2013).

[23] S. Jain, V. Novosad, F. Y. Fradin, J. E. Pearson, and S. D. Bader, Dynamics of coupled vortices in perpendicular field, Appl. Phys. Lett. **104**, 082409 (2014).

[24] S. I. Kiselev, J. C. Sankey, I. N. Krivorotov, N. C. Emley, R. J. Schoelkopf, R. A. Buhrman, and D. C. Ralph, Microwave oscillations of a nanomagnet driven by a spin-polarized current, Nature **425**, 380 (2003).

[25] S. Kaka, M. R. Pufall, W. H. Rippard, T. J. Silva, S. E. Russek, and J. A. Katine, Mutual phase-locking of microwave spin torque nano-oscillators, Nature **437**, 389 (2005).

[26] S. E. Russek, W. H. Rippard, T. Cecil, and R. Heindl, Spin-Transfer Nano-Oscillators, in *Handbook of Nanophysics: Functional Nanomaterials*, edited by K. D. Sattler (CRC Press, Boca Raton, FL, 2010), pp. 1–23.

[27] R. Lebrun, N. Locatelli, S. Tsunegi, J. Grollier, V. Cros, F. A. Araujo, H. Kubota, K. Yakushiji, A. Fukushima, and S. Yuasa, Nonlinear behavior and mode coupling in spin-transfer nano-oscillators, Phys. Rev. Applied **2**, 061001 (2014).

[28] D. Li, Y. Zhou, C. Zhou, and B. Hu, Global attractors and the difficulty of synchronizing serial spin-torque oscillators, Phys. Rev. B **82**, 140407 (2010).

[29] G. Csaba, M. Pufall, W. Rippard, and W. Porod, Modeling of coupled spin torque oscillators for applications in associative memories, in *Proceedings of the 12th IEEE Conference on Nanotechnology (IEEE-NANO)* (IEEE, New York, 2012), pp. 1–4.

[30] G. Csaba, M. Pufall, D. E. Nikonov, G. I. Bourianoff, A. Horvath, T. Roska, and W. Porod, Spin torque oscillator models for applications in associative memories, in *Proceedings of the 13th International Workshop on Cellular Nanoscale Networks and Their Applications (CNNA)* (IEEE, New York, 2012), pp. 1–2.

[31] T. Roska, A. Horvath, A. Stubendek, F. Corinto, G. Csaba, W. Porod, T. Shibata, and G. Bourianoff, An associative memory with oscillatory cnn arrays using spin torque oscillator cells and spin-wave interactions architecture and end-to-end simulator, in *Proceedings of the 13th International Workshop on Cellular Nanoscale Networks and Their Applications (CNNA)* (IEEE, New York, 2012), pp. 1–3.

[32] T. Shibata, R. Zhang, S. P. Levitan, D. E. Nikonov, and G. I. Bourianoff, Cmos supporting circuitries for nano-oscillator-based associative memories, in *Proceedings of the 13th International Workshop on Cellular Nanoscale Networks and Their Applications (CNNA)* (IEEE, New York, 2012), pp. 1–5.

[33] F. B. Mancoff, N. D. Rizzo, B. N. Engel, and S. Tehrani, Phase-locking in double-point-contact spin-transfer devices, Nature **437**, 393 (2005).

[34] B. Georges, J. Grollier, M. Darques, V. Cros, C. Deranlot, B. Marcilhac, G. Faini, and A. Fert, Coupling efficiency for phase locking of a spin transfer nano-oscillator to a microwave current, Phys. Rev. Lett. **101**, 017201 (2008).

[35] J. Shibata, K. Shigeto, and Y. Otani, Dynamics of magnetostatically coupled vortices in magnetic nanodisks, Phys. Rev. B **67**, 224404 (2003).

[36] A. Vogel, A. Drews, T. Kamionka, M. Bolte, and G. Meier, Influence of dipolar interaction on vortex dynamics in arrays of ferromagnetic disks, Phys. Rev. Lett. **105**, 037201 (2010).

[37] A. Awad, G. Aranda, D. Dieleman, K. Y. Guslienko, G. N. Kakazei, B. A. Ivanov, and F. G. Aliev, Spin excitation frequencies in magnetostatically coupled arrays of vortex state circular permalloy dots, Appl. Phys. Lett. **97**, 132501 (2010).

[38] A. Barman, S. Barman, T. Kimura, Y. Fukuma, and Y. Otani, Gyration mode splitting in magnetostatically coupled magnetic vortices in an array, J. Phys. D: Appl. Phys. **43**, 422001 (2010).

[39] H. Jung, Y.-S. Yu, K.-S. Lee, M.-Y. Im, P. Fischer, L. Bocklage, A. Vogel, M. Bolte, G. Meier, and S.-K. Kim, Observation of coupled vortex gyrations by 70-ps-time- and 20-nm-space-resolved full-field magnetic transmission soft x-ray microscopy, Appl. Phys. Lett. **97**, 222502 (2010).

[40] H. Jung, K.-S. Lee, D.-E. Jeong, Y.-S. Choi, Y.-S. Yu, D.-S. Han, A. Vogel, L. Bocklage, G. Meier, M.-Y. Im, P. Fischer, and S.-K. Kim, Tunable negligible-loss energy transfer between dipolar-coupled magnetic disks by stimulated vortex gyration, Sci. Rep. **1**, 59 (2011).

[41] D. V. Berkov, Synchronization of spin-torque-driven nano-oscillators for point contacts on a quasi-one-dimensional nanowire: Micromagnetic simulations, Phys. Rev. B **87**, 014406 (2013).

[42] A. Dussaux, B. Georges, J. Grollier, V. Cros, A. Khvalkovskiy, A. Fukushima, M. Konoto, H. Kubota, K. Yakushiji, S. Yuasa, K. A. Zvezdin, K. Ando, and A. Fert, Large microwave generation from current-driven magnetic vortex oscillators in magnetic tunnel junctions, Nat. Commun. **1**, 8 (2010).

[43] A. V. Khvalkovskiy, J. Grollier, A. Dussaux, K. A. Zvezdin, and V. Cros, Vortex oscillations induced by spin-polarized current in a magnetic nanopillar: Analytical versus micromagnetic calculations, Phys. Rev. B **80**, 140401 (2009).

[44] K. Guslienko, B. Ivanov, V. Novosad, Y. Otani, H. Shima, and K. Fukamichi, Eigenfrequencies of vortex state excitations in magnetic submicron-size disks, J. Appl. Phys. **91**, 8037 (2002).

[45] In the two-vortex ansatz model the volume-averaged magnetization of the shifted vortex is proportional to its displacement $\mu/V = \langle \mathbf{M}(\mathbf{X}(t))\rangle_V = -\xi C M_s/R[\mathbf{z}\times\mathbf{X}(t)]$, where $V = \pi R^2 h$, $\mathbf{X}(t) = X[\cos(\varphi(t)), \sin(\varphi(t))]$ and $\xi = 2/3$ for this model [44,53].

[46] A. A. Thiele, Steady-state motion of magnetic domains, Phys. Rev. Lett. **30**, 230 (1973).

[47] Y. Gaididei, V. P. Kravchuk, and D. D. Sheka, Magnetic vortex dynamics induced by an electrical current, Int. J. Quantum Chem. **110**, 83 (2010).

[48] K. Y. Guslienko, X. F. Han, D. J. Keavney, R. Divan, and S. D. Bader, Magnetic vortex core dynamics in cylindrical ferromagnetic dots, Phys. Rev. Lett. **96**, 067205(R) (2006).

[49] B. A. Ivanov and C. E. Zaspel, Excitation of spin dynamics by spin-polarized current in vortex state magnetic disks, Phys. Rev. Lett. **99**, 247208 (2007).

[50] A. Dussaux, A. V. Khvalkovskiy, P. Bortolotti, J. Grollier, V. Cros, and A. Fert, Field dependence of spin-transfer-induced vortex dynamics in the nonlinear regime, Phys. Rev. B **86**, 014402 (2012).

[51] A. Chanthbouala, R. Matsumoto, J. Grollier, V. Cros, A. Anane, A. Fert, A. V. Khvalkovskiy, K. A. Zvezdin, K. Nishimura, Y. Nagamine, H. Maehara, K. Tsunekawa, A. Fukushima, and S. Yuasa, Vertical-current-induced domain-wall motion in MgO-based magnetic tunnel junctions with low current densities, Nat. Phys. **7**, 626 (2011).

[52] SPINPM is a micromagnetic code developed by the Istituto P.M. srl, Torino, Italy (www.istituto-pm.it) based on a fourth-order Runge-Kutta numerical scheme with an adaptative time-step control for the time integration.

[53] K. Guslienko, Low-frequency vortex dynamic susceptibility and relaxation in mesoscopic ferromagnetic dots, Appl. Phys. Lett. **89**, 022510 (2006).